doi.org/10.26434/chemrxiv.11328173.v1

Assembly and Characterization of Polyelectrolyte Complex Micelles

Alexander Marras, Jeffrey Vieregg, Matthew Tirrell

Submitted date: 05/12/2019 • Posted date: 13/12/2019

Citation information: Marras, Alexander; Vieregg, Jeffrey; Tirrell, Matthew (2019): Assembly and Characterization of Polyelectrolyte Complex Micelles. ChemRxiv. Preprint. https://doi.org/10.26434/chemrxiv.11328173.v1

We provide protocols and representative data for designing, assembling, and characterizing polyelectrolyte complex micelles (core-shell nanoparticles formed by polyelectrolytes and hydrophilic charged-uncharged block copolymers).

File list (1)

Revised version_preprint.pdf (12.21 MiB) view on ChemRxiv • download file

Assembly and Characterization of Polyelectrolyte Complex Micelles

Alexander E. Marras[1], Jeffrey R. Vieregg[1], Matthew V. Tirrell[1]

[1]Pritzker School of Molecular Engineering, The University of Chicago, Chicago, IL, USA

Abstract

Polyelectrolyte complex micelles (PCMs), core-shell nanoparticles formed by self-assembly of charged polymers in aqueous solution, provide a powerful platform for exploring the physics of polyelectrolyte interactions and also offer a promising solution to the pressing problem of delivering therapeutic oligonucleotides in vivo. Developing predictive structure-property relationships for PCMs has proven difficult, in part due to the presence of strong kinetic traps during nanoparticle self-assembly. This article discusses criteria for choosing polymers for PCM construction and provides protocols based on salt annealing that enable assembly of repeatable, low-polydispersity nanoparticles. We also discuss PCM characterization using light scattering, small-angle X-ray scattering, and electron microscopy.

Introduction

When oppositely charged polyelectrolytes are mixed in aqueous solution, entropy gain from release of their counterions causes demixing of the solution into a polymer-rich condensed phase and a polymer-depleted supernatant[1-5], a phenomenon known as polyelectrolyte complexation. If a neutral hydrophilic block is conjugated to one or both of the polyelectrolytes, nano-scale phase separation occurs instead (Figure 1A). The resulting self-assembled core-shell nanoparticles are variously referred to as polyelectrolyte complex micelles (PCMs), polyion complex micelles, block ionomer complexes, or coacervate-core micelles by analogy to surfactant micellization, even though all components of the system are hydrophilic[6,7]. PCMs' ability to encapsulate hydrophilic molecules such as proteins and nucleic acids, as well as the extensive tunability offered by the block copolymer carrier architecture makes them attractive candidates for delivering therapeutic molecules in vivo[8-13].

Delivering therapeutic nucleic acids to cellular targets is a particularly important challenge, and one for which PCMs offer several advantages. Therapeutic nucleic acids (genetic DNA, messenger RNA, and oligonucleotides such as siRNA) have immense potential for improving human health, but must overcome numerous biological and physical barriers to realize that potential[14-16]. Bare nucleic acids are degraded by serum and cellular nucleases and are also quickly cleared from circulation, while their strong negative charge makes it difficult for them to penetrate cell membranes without assistance. Current approaches for overcoming these barriers include costly chemical modifications to prevent attack from nucleases and/or encapsulation into various lipid nanoparticles assembled via hydrophobic interactions[15,17,18]. While these methods have proven effective for local injections and liver targeting, systemic use presents significant limitations of toxicity, immunogenicity, and limited biodistribution[16]. By contrast, PCMs use the negative charge of nucleic acids to condense them within the phase-separated

core, while the neutral corona provides a steric barrier against degradation as well as a platform for incorporating ligands to enhance targeting or internalization[11,19]. In vitro and animal studies have shown that PCMs can effectively deliver various nucleic acid payloads[20-24], but weaknesses in our ability to predict PCM properties such as size, shape, and stability from the properties of the constituent polymers have hindered their wider adoption.

Recent work by our group and others in the field has begun to address this problem by developing structure-property, and in some cases structure-property-function relationships for PCMs formed from nucleic acids and various cationic-neutral polymers[7,25-27]. Two consistent themes that have emerged from these studies are the importance of developing well-controlled, repeatable protocols for PCM assembly and the benefit of using multiple techniques to characterize the resulting nanoparticles. Polyelectrolytes, particularly those with high charge density like nucleic acids, interact with each other very strongly, and appear to readily become kinetically trapped upon mixing, resulting in PCM preparations that are highly sensitive to small variations in procedure and display high polydispersity and poor repeatability from batch to batch. PCMs have also been shown to adopt a wide range of shapes and sizes depending on the atomic-level configurations of their components, and capturing this diversity with any individual characterization technique is very difficult, particularly since some common techniques such as dynamic light scattering (DLS) require assumptions about particle shape to interpret.

In this article, we discuss materials design and selection for PCMs, with a focus on oligonucleotides and cationic-neutral diblock copolymers. We then describe a “salt annealing” protocol that uses high salt concentrations followed by slow dialysis to avoid kinetic trapping during PCM assembly. The polyelectrolytes are mixed in high salt conditions where electrostatic attractions are screened, then the salt concentration is slowly lowered to allow the polyelectrolytes to settle into their most energetically favorable configurations, analogous to the slow cooling process of thermal annealing. Using this protocol, we are regularly able to achieve exceptionally low polydispersity and high repeatability for oligonucleotide PCMs[7,26]. Finally, we describe how four separate measurement techniques can be used to characterize PCMs over a very wide range of length scales, from external morphology to internal structure: DLS, multi-angle light scattering (MALS), small angle X-ray scattering (SAXS), and transmission electron microscopy (TEM). We hope that these protocols will enable more researchers to effectively explore the capabilities of these interesting nanoparticles.

Polymer selection and preparation

PCM properties are strongly influenced by the physical and chemical characteristics of the constituent polymers, making polymer selection a critical step in the design process. The most well-characterized block copolymers for nucleic acid PCMs are linear diblocks such as poly(lysine)-poly(ethylene glycol) (pLys-PEG), but PCMs can be formed between polyelectrolytes and a variety of hydrophilic neutral-charged polymers, which can be

generated in a high throughput manner[28]. The choice of charged group strongly affects the stability of ion pairing and shape of micelles[26], and PCM size has been shown to increase with the length of the charged block[5,7,26] (Figure 2), thus allowing PCM properties to be tuned for the requirements of a desired application. For linear diblocks, we have found that the charged block should have at least 10 charges and be strongly charged at the desired pH. Longer charged blocks (we have successfully observed PCM formation with block lengths up to 200, and the literature describes longer polymers) may promote PCM formation with oligonucleotides such as siRNA that are difficult to complex with shorter blocks[21]. More flexibility is available in the choice of neutral block[24], but experience has shown that very short neutral blocks lead to aggregation rather than nanoparticle formation, and that the minimum neutral length increases with charged block length. For pLys-PEG, a PEG MW of at least 3000-5000 is required for pLys lengths below ~50, and longer lengths are required as the charged block is increased further. Increased neutral block length results in increased PCM size, particularly shell thickness due to steric crowding of the neutral polymers.

This manuscript presents a protocol for preparing PCMs from lyophilized high-purity pLys-PEG and oligonucleotides of known quantity, but should be readily adaptable to other systems as well; we have tested it successfully with several charged polypeptides (poly(arginine), poly(glutamic acid)) as well as several synthetic polyelectrolytes (poly(acrylic acid), poly(vinylbenzyl trimethylammonium)). We also describe preparing PCMs with a stoichiometric ratio of polyelectrolyte charges, but this is easily modified. We find it easiest to work in charge concentration units (c.c.), which also naturally accommodates polymers that are not fully charged. If either polymer is not well-characterized, care should be taken to accurately determine the polymer lengths/masses and ensure that excess salt is not present beyond that needed for charge neutralization, e.g. by dialysis. The presence of any retained water should also be accounted for when concentrations are calculated. Nucleic acid concentration can be conveniently quantified by 260 nm absorbance, and the presence or absence of terminal phosphates should be considered when calculating the charge concentration.

When using oligonucleotides as a polyanion, the hybridization state and chemical structure help determine the propensity for self-assembly and the characteristics of the resulting PCM[5,7,26]. Optimizing these, within the requirements for biological efficacy (if using PCMs for delivery) will increase the likelihood of forming the desired structures. Helpful tools for analyzing hybridization include MATLAB functions for nucleic acids, NUPACK[29], and IDT OligoAnalyzer. We recommend analyzing a candidate sequence to understand the strength of binding to 1) itself in a hairpin formation, 2) another copy of the same sequence (self-dimer), and 3) to other oligonucleotides present in the system. DNA and RNA melting temperatures for a specific sequence can also be calculated using the nearest-neighbor method[30,31]. Thermal annealing of nucleic acids (Step 2.3) denatures any residual secondary structure in the individual nucleotides and promotes equilibrium folding.

PCM Characterization and Analysis

A wide range of techniques are available for characterizing nanoparticles, including static and dynamic light scattering, small angle scattering of electrons or neutrons, and electron microscopy. In this article, we provide protocols for two light scattering techniques, small angle X-ray scattering, and two electron microscopy techniques.

Dynamic light scattering (DLS) measures the autocorrelation of temporal fluctuations in scattering intensity at one angle from Brownian motion of the sample. Fitting this data can provide hydrodynamic radius and polydispersity for spherical micelles (Figure 3). Multiple angle light scattering (MALS) measures the static scattering intensity at many angles; this angular dependence reports on the shape of the nanoparticle but is limited to length scales longer than ~50 nm for visible light, which limits its effectiveness for smaller nanoparticles. Both techniques are based on refractive index mismatch and report primarily on the outside dimensions of the nanoparticle.

Small angle X-ray scattering (SAXS) uses X-rays as the scattering probe, and their shorter wavelength allows measurements over a range of ~0.1 – 100 nm. Fitting the observed scattering intensity vs angle (conventionally expressed as momentum transfer q) provides information on PCM morphology (size and shape) and also internal structure. If absolute intensity calibration is available, and if the scattering intensity can be extrapolated to zero angle, PCM mass and aggregation number can also be estimated[32], making SAXS an extremely versatile and valuable method. Small angle neutron scattering (SANS) is sensitive over a similar range of length scales, but is only available at specialized facilities and will not be explicitly discussed in this article[33-35].

Recent years have seen the advent of benchtop SAXS instruments, but we find that synchrotron sources are better suited for PCM characterization, as their higher intensity allows data to be collected much faster for these low-contrast samples. We provide a brief protocol for acquiring PCM SAXS data at Beamline 12-ID-B at the Advanced Photon Source (Argonne National Laboratory, USA) from a user perspective. This protocol should be applicable to most synchrotron sources but consulting with local staff before proposing an experiment is highly recommended. We also provide a data reduction and analysis protocol using Irena[36], a free set of macros written for Igor Pro. Irena includes a versatile set of form factors for modeling SAXS data and allows for construction of multi-component models that are capable of describing the complex scattering profile of PCMs (see Representative Results, Figure 4). Irena also has a fairly comprehensive set of documentation and tutorials available online. Before attempting the procedures below, we recommend familiarizing yourself with these, particularly the tutorial ‘Modeling of SAXS data with two main scatterer populations’.

Radiation damage is a concern for X-ray scattering, but several measures can be employed to minimize this. In particular, we recommend using a flow cell setup with a syringe pump and PCM sample flowing during data acquisition, rather than a sealed capillary; this also greatly simplifies background subtraction. We also suggest taking

multiple exposures of the flowing sample rather than one longer one in order to limit the flux that any single volume of sample sees and to allow for comparison of the exposure data to identify any damage that may occur.

In contrast to the scattering techniques, which generally require fitting to interpret, transmission electron microscopy (TEM) provides a real-space visual image of the nanoparticles by passing an electron beam through the sample and projecting an image on a scintillation screen (Figure 5). We present protocols for two TEM techniques in this article. Cryo TEM freezes micelle samples into a thin layer of vitreous ice, preserving structural conformation with minimal foreign substances, optimal for micelles ≤~10-100nm in radius. Negative stain TEM uses a heavy metal salt (e.g. uranium) to surround the sample after it has been dried on the surface of a grid. The dense stain will scatter more electrons than the sample, adding contrast and producing a negative image of the sample. Cryo TEM is recommended for high quality images, however, it is more costly, time consuming, and may not provide sufficient contrast. When this is a concern, negative stained samples should be used. Examples of each are shown in Figure 5.

Each of these techniques reports on slightly different aspects of the nanoparticles, with different strengths and limitations. Light scattering is readily available, and is often the fastest approach, but has substantial limitations in size and shape resolution. SAXS can provide information over a large range of length scales at reasonably high throughput, but requires specialized equipment to acquire the data, as well as modeling to interpret it. TEM images are straightforward to interpret but can be limited in contrast and are inherently low throughput. Our experience has shown that using multiple techniques for characterization greatly increases the information that can be obtained about PCM properties and simplifies interpretation of the sometimes underdetermined data sets obtained from each one alone. For example, SAXS and TEM primarily interrogate PCMs' dense cores, while light scattering reports on the overall dimensions of the nanoparticle; combining them thus allows measurement of both core and corona size. TEM's ability to acquire real space images can provide 'ground truth' data to enable selection of appropriate form factors for modeling SAXS data that might otherwise be ambiguous. This article describes protocols for all four techniques, and an example process for using them to characterize an unknown sample is given in the Discussion section.

Protocol

1 Preparation of Materials

1.1 Weigh out lyophilized diblock polymer and add water up to nearly the volume required for a stock solution of 10 mg/mL final concentration. Vortex at max speed for 2 min.

1.2 Sonicate for 5 min. Very long diblocks may require additional sonication. The stock solution should appear completely transparent and homogeneous.

1.3 Adjust pH to 7.4 using NaOH or HCl as needed. Add water to final volume. pLys-PEG solutions are fairly stable, but should be refrigerated for longer-term storage and pH checked before use. Lyophilization is preferable to freezing.

1.4 Resuspend lyophilized oligonucleotide(s) at desired stock concentration (typically 2-5 mM molecular concentration for lengths of 50 nt or below). Vortex thoroughly to ensure full dissolution.

1.5 Calculate molar concentrations using MW or length as described above.

1.6 Calculate molar charge concentration (c.c.), where

$$c.c. = (molecular\ concentration) \times (charge)$$

The polyelectrolyte charge is the number of charged monomers, while the nucleic acid charge is the number of bases minus 1, assuming no phosphorylation. Keep in mind that double-stranded DNA will have twice as many charges per molecule compared to single-stranded DNA.

1.7 Create diluted stock at 20 mM c.c. for each polymer.

2 Nucleic Acid Polyelectrolyte Micelle Preparation

2.1 Mix the following in a 1.5 mL microcentrifuge tube (280 µL total):

2.1.1 200 µL of Nuclease-free water (ultrapure water for PCMs not containing nucleic acids).

2.1.2 40 µL of 10x PBS (phosphate-buffered saline: 137 mM NaCl, 10 mM phosphate, pH 7.4 when diluted to 1x) or other suitable buffer[37].

2.1.3 40 µL of 20 mM c.c. oligonucleotide. For double-stranded oligonucleotides, add 20 µL of each strand at 20 mM c.c..

2.2 Incubate 5 min @ 70°C. If the calculated melting temperature for the oligonucleotides is higher, this temperature should be increased accordingly. Note that RNA will degrade at elevated temperatures, so this step should not be unduly lengthened if this or other sensitive components are present.

2.3 Cool on bench 15 min.

2.4 Add 40 µL of 20 mM c.c. diblock, vortex immediately for 20 s at max speed.

2.5 Incubate 5 min at room temperature.

2.6 Perform salt anneal

2.6.1 Add 80 µL of 5M NaCl, for a final concentration of 1M NaCl. Vortex 10 s at max speed

2.6.2 Incubate 10 min, then load into dialysis cartridges. Note that the listed MW cutoffs are determined for globular proteins and will not be accurate for linear

polymers. We find that a 2k MWCO cartridge avoids sample loss and also provides for gradual changes in ionic strength.

2.6.3 Prepare dialysis baths

2.6.3.1 Calculate sufficient volume of dialysis bath:

$$(\text{number of samples}) \times \left(400 \frac{\mu\text{L}}{\text{sample}}\right) \times (300\text{x})$$

2.6.3.2 Mix 10x PBS or other desired buffer, 5M NaCl, and ultrapure water for a final solution of 1x PBS and 0.5M NaCl, as well as two solutions of 1x PBS.

2.6.4 Load dialysis cartridges

2.6.4.1 Label cartridges with permanent marker. Soak cartridges in buffer for at least 2 min to hydrate membranes.

2.6.4.2 Remove cap by twisting counter-clockwise. Load sample using gel loading pipette tip. Remove excess air by gently squeezing membranes. Replace cap.

2.6.4.3 Put cartridges in 0.5M NaCl + 1x PBS bath. Cartridges should float, with both membranes exposed to the bath. Foam floats can be used to ensure this if needed.

2.6.5 Dialysis

2.6.5.1 Incubate for 24 h stirring slowly with a magnetic stir bar.

2.6.5.2 Move cartridges to a new bath of 1x PBS or other desired working buffer. Incubate for 24 h stirring slowly with a magnetic stir bar.

2.6.5.3 Repeat previous step with a new bath of 1x PBS or other desired working buffer.

2.6.6 Recover Sample

2.6.6.1 Remove cartridges from bath.

2.6.6.2 Remove cap and recover sample using gel loading pipette tip. Note that recovered volume may be higher than initial 400 µL due to membrane swelling. Record recovered volume if slight dilution is a concern.

2.6.6.3 Place sample into clean 1.5 mL microcentrifuge tube. PCMs prepared in this way should be stable for several months when refrigerated, provided that nuclease contamination has been avoided.

Characterization and Analysis:

3 Dynamic Light Scattering

3.1 To ensure dust-free conditions, buffers should be carefully filtered (3x filtered through an 0.22 µm syringe or vacuum filter) and glassware thoroughly cleaned

between samples. It is also important to ensure that the sample has reached thermal equilibrium before conducting the measurement.

3.2 Dilute the PCM sample to 0.2 mM c.c. (10x if using the protocol described above) with the desired working buffer and load into a suitable cuvette. We use a small-volume cuvette, which requires ~200 µL of sample after dilution.

3.3 Set DLS detector position to 90 degrees.

3.4 Adjust the laser power and/or attenuator so the count rate is 100-200k counts per second (cps), if possible. Count rates as low as 10 kcps can be used, but measurement times may need to be extended to obtain good statistics (step 4.1). Higher count rates should be avoided, as multiple scattering will confound the measurement.

3.5 Acquire data for 1 minute. The count rate should be constant over the entire acquisition time; if not, this indicates that some component of the sample or instrument has not yet equilibrated.

3.6 Examine the autocorrelation data. The long-time baseline should be very flat, and the autocorrelation curve should be smooth, with minimal scatter, as shown in Figure 3A. Baseline drift indicates lack of equilibrium, and noise in the data can be improved by acquiring more data.

3.7 Fit autocorrelation function

3.7.1 REPES[38,39] performs regularized inverse Laplace transformation to deliver a distribution of relaxation times and a diffusion coefficient, *D*. It then calculates hydrodynamic radius, R_h, using the Stokes-Einstein equation: $R_h = k_B T / 6\pi\eta D$. Figure 1B shows representation of R_h and Figure 3B shows the result of REPES.

3.7.2 Alternative methods include CONTIN[40,41] (an alternative regularization algorithm) or non-negative least-squares fitting (NNLS). Consistent results from multiple fitting methods is a signature of high-quality data. Note that cumulant analysis (standard on many instruments) gives non-physical values for multimodal size/length distributions.

4 Multi-Angle Light Scattering

Light scattering intensity vs angle can be measured on a variety of instruments. We have obtained good results using both goniometer-based instruments and multiple-detector instruments, run in batch mode.

4.1 Adjust PCM concentration and illumination intensity to provide sufficient signal/noise (vs. a buffer-only sample) at all angles without saturating any detector. The latter can be tested by preparing samples at various dilution factors and checking for linearity of intensity vs concentration (assuming minimal interaction between PCMs).

4.2 Record the light scattering rate from 15-135° for 1 minute per angle. If the sample and instrument are properly equilibrated, the scattering rate will be constant over the measurement time.

4.3 Plot the normalized scattering rate $I \sin\theta$ vs. q, where I is the scattering rate. q is the scattering vector (photon momentum transfer) as defined by

$$q = 4\pi\eta \sin(\frac{\theta}{2})/\lambda$$

where η = solvent refractive index, θ = measurement angle, and λ = wavelength of the light source. Figure 4 shows a plot of MALS scattering intensity.

5 Small Angle X-ray Scattering

5.1 Data Acquisition

5.1.1 Prepare PCM samples as described above at 2 mM charge concentration for oligonucleotide PCMs for ample scattering above background. For PCMs lacking heavy atoms (e.g. phosphorous in nucleic acids), higher concentrations may be required. Scattering length densities can be estimated using calculators such as SASSIE[42].

5.1.2 In order to minimize radiation damage by scavenging free radicals, add glycerol from a concentrated (e.g. 50%) stock solution so that micelle solution contains 1% (v/v) glycerol. Note that neat glycerol is highly viscous and difficult to accurately measure. Diluting with water or buffer is highly recommended.

5.1.3 Also prepare a large volume of working buffer with 1% glycerol for use as a background monitor.

5.1.4 Prepare flow cell apparatus (beamline specific; we typically use a 3 mm diameter quartz capillary connected to a computer-controlled syringe pump with small diameter, minimal length polyethylene tubing) and calibrate detector. We find that a minimum volume of ~140 µL per sample is needed with our setup.

5.1.5 Determine sample exposure parameters. The optimum exposure will vary based on beam intensity, detector sensitivity, and the concentration, scattering strength, and damage susceptibility of the sample), but the goal is to expose the sample to the minimal flux required to obtain sufficient scattering intensity over the q-range of interest.

5.1.6 For oligonucleotide + pLys-PEG PCMs, we find that 30x 0.2 s exposures at a 1 Hz repetition rate produces good data quality with little perceptible damage. For new samples, this procedure may be helpful:

5.1.6.1 Prepare PCM samples over a range of concentrations (e.g. 10 – 10,000 µM c.c.).

5.1.6.2 Starting at an intermediate concentration, alternate PCM and buffer-only samples with varying exposure times. See below for data acquisition and reduction procedure. Sample signal should have good statistics (small statistical error, or smooth variation across q), If the statistics are poor, the exposure time may be increased.

5.1.6.3 Sample signal should also be clearly distinguishable from background over the q range of interest. Compute and plot the (signal – background)/background ratio vs q to determine signal/background ratio. If the signal/background ratio is low, sample concentration should be increased.

5.1.6.4 Verify that the scattering intensity (normalized to concentration) is independent of sample concentration by acquiring data at higher and lower concentrations, scaling exposure time if needed. Interparticle interactions (the most likely cause of concentration dependence) will be most pronounced in the low q range.

5.1.7 Acquire data for PCM samples and background (buffer + glycerol):

5.1.7.1 Trigger syringe pump to move sample through the capillary. Either bidirectional or once-through motion is acceptable, but care should be taken to isolate each sample, e.g. by inserting an air bubble between samples. Samples may be recovered and can be re-used if no radiation damage is seen.

5.1.7.2 Once flow has started, trigger X-ray exposure and data acquisition program (described above). Care should be taken that beam exposure ends before fluid flow does.

5.1.8 After each sample, perform azimuthal averaging and plot the 1D (intensity vs. q) profiles for each exposure together. They should be identical within statistical error; changing signal over time can indicate radiation damage.

5.1.8.1 Isolated anomalous profiles may indicate the presence of microbubbles. If bubbles are observed frequently, decreasing the flow rate may help.

5.1.9 Average the 1D scattering profiles.

5.1.10 Acquire data for buffer-only samples frequently (once per every 4-5 PCM samples) and compare these over time. Increased signal from buffer-only samples is indicator that the capillary may be becoming fouled from radiation-damaged sample.

5.1.10.1 When fouling is noticed, wash the capillary with bleach, and consider reducing exposure time if possible.

5.2 Data reduction and analysis using Irena

5.2.1 Import micelle and background ASCII data sets (SAS/Data import export/Import ASCII SAS data).

5.2.2 Subtract background scattering from sample data. Typically, the highest q values (e.g. $q > 0.5$) show incoherent scattering from the solvent dominates the signal. Scaling the background data to match the sample data over this q-range removes any variation due to beam intensity variation and sample concentration.

5.2.2.1 Plot sample and background together on a log-log scale. Verify flat intensity at high q (SAS/Data Manipulation/Data Manipulation I). Compute (sample/background) ratio (Data1/Data 2), plot on a linear-log scale, and verify high-q asymptote.

5.2.2.2 Compute the average (sample/background) ratio over this q range (custom Igor macro or copy/paste into Excel from the Igor Data Browser).

5.2.2.3 Using the Data Manipulation macro, scale the background (e.g. Modify Data 2) using the ratio computed above and plot the ratio of background-subtracted signal to background vs q ([Data1-Data2]/Data2), verifying that it now asymptotes to zero at high q. Record this ratio; it should be <1-2 percent away from 1.0 for each sample.

5.2.2.4 Plot the background-subtracted signal (Data1-Data2) vs q, and save the data with a new name. Do not overwrite the original data.

5.2.2.5 If high-q data is not available, use a scaling factor of 1 for background subtraction, but be aware that inaccuracies may be introduced in q ranges where the signal/background ratio is small.

5.2.3 Open the Modeling macro, (SAS/Modeling), load and plot the background-subtracted data (Data cntrls/Add data; do not scale in this macro).

5.2.4 First, find an approximate model for the external surface of the PCM (micelle size/shape):

5.2.4.1 In Data cntrls, select low to moderate q range (e.g. ~0.003Å^{-1} < *q* < ~0.1Å^{-1}). If oscillations are visible, include them.

5.2.4.2 Choose a form factor appropriate for your data. The slope at low q is indicative of nanoparticle shape, which can also be verified through TEM and/or MALS. We generally use Schulz-Zimm spheroid (q^0), cylinder (q^{-1}), or flexible cylinder (q^{-2}) models. Irena provides tools for fitting power laws (SAS/Support Tools for plots and tables).

5.2.4.3 In Model cntrls, select the first scattering population (1P) and make sure it is the only one in use (Select 'Use?' checkbox).

5.2.4.4 Select 'Size dist.' for Model and choose the desired Distribution type and Form Factor. Set initial parameters for the search by entering values in the Scale, Mean Size and Width fields and clicking 'Calculate Model' to draw the resulting form factor.

5.2.4.5 Once reasonable parameters have been found, click 'Fit Model' to perform a nonlinear least-squares fit to the data. The 'Size distribution' model gives mean radius and width.

To calculate polydispersity (PDI):

$$PDI = (stdev/radius)^2 = [(width^2)/4]/(radius^2)$$

As with any nonlinear fitting procedure, it may be necessary to adjust the data range (q region) and starting parameters in order to obtain a stable, physically reasonable fit.

5.2.4.6 Once a reasonable fit is obtained, save it (Store in Notebook/Store in Folder).

5.2.5 Second, consider the individual polymers within the PCM core also scatter X-rays, which can be captured by a power law model (e.g. q^{-2} for ideal chains, $q^{-5/3}$ for swollen chains, etc.). Irena implements this through a Beaucage model[43]: $I(q) = Gexp(-q^2{R_g}^2/3) + B\{[\mathrm{erf}\,(qR_g/6^{1/2})]^3/q\}^P$ where P is the power law and G and B are prefactors.

5.2.5.1 Adjust the data controls to cover the entire q range and replot the model (Calculate Model). Typically, excess scattering will be observed in the moderate to high q range (e.g. $q > \sim 0.1$Å^{-1}).

5.2.5.2 Use the data controls to select the q range where excess scattering (> 10x the form factor model) is observed.

5.2.5.3 Add a second scattering population (2P) and make sure it is the only one in use (deselect 'Use?' for 1P).

5.2.5.4 Select 'Unified level' for model. B and P are the relevant parameters here. Use the plotting support tools or the 'Fit P/B between csrs' macro to obtain an initial guess for these parameters, and adjust the Guinier factors G and R_g to ensure that the model does not predict excessive scattering at low q.

5.2.5.5 As for the form factor, perform a nonlinear fit and record the parameters and model.

5.2.6 Third, if a diffraction peak is present, as in Figure 4, add a third model for a diffraction peak in the q range of interest (q~0.22Å^{-1} in this case).

5.2.7 Once approximate fit values are obtained for the individual scattering populations, turn on all three together (select 'Use?" for each) and optimize the combined fit.

5.2.8 Check that each value remains physically reasonable. The result of this procedure should be a composite model that describes the SAXS data well over a large range of size scales, as illustrated in Figure 4.

5.2.9 Save fit in Igor folder.

6 Transmission Electron Microscopy (TEM)

6.1 Cryo TEM

6.1.1 Select grid. We recommend holey carbon support film on a standard TEM grid or lacey carbon as an alternative. In either case the holes between the carbon will provide an imaging area of pure vitreous ice and sample and no film.

6.1.2 Place the grid carbon-side up in a glow discharging apparatus on a clean glass slide. Wrapping the slide in laboratory film can help with grid handling. Avoid touching the center of grid with tweezers and always pinch near the edge of the grid.

6.1.3 Expose grid for 30 s.

6.1.4 Prepare a vitrification robot for sample deposition.

6.1.4.1 Set to 100% humidity and room temperature and add blotting paper. Prepare liquid ethane and liquid nitrogen baths at the base of the robot. See online tutorials and videos for additional help with vitrification robot preparation and use.

6.1.5 Dilute sample 5x.

6.1.6 Using the negative-action tweezers provided with the vitrification robot, pick up a grid then attach the tweezers to the robot and move the tweezers into the chamber.

6.1.7 While in the robot, add 4 µL of sample to the carbon side of grid using a pipette through the hole in the side of the machine.

6.1.8 Incubate for 4 min.

6.1.9 Using the robot, blot 3-5 s with filter paper.

6.1.10 The vitrification robot will plunge the grid into liquid ethane.

6.1.11 Remove the tweezers and move the grid to liquid nitrogen and into a storage container, which should also be under liquid nitrogen. This process fixes the sample into a thin layer of vitreous ice. Minimize the time the grid spends out of liquid ethane or liquid nitrogen during this step.

6.1.12 Cool the cryo sample holder using liquid nitrogen. Keep the dewar and reservoir full.

6.1.13 When ready to image, load the grid onto the cryo sample holder. Keep the sample under liquid nitrogen or briefly in the extremely cold nitrogen steam just above liquid surface.

6.1.14 Image grid at 120 kV between 75kx and 150kx in thin and thick ice, as different sized micelles may prefer a certain ice thickness.

6.1.14.1 Limit beam exposure to avoid melting ice and damaging the sample. Do not focus directly where you plan to image (do it somewhere nearby). Only expose the area of interest while capturing an image.

6.1.14.2 Be sure to differentiate liquid ethane drops from sample when viewing images (see Figure 5).

6.2 Conventional TEM using negative staining

6.2.1 Prepare Stain

6.2.1.1 Boil ~10 mL of ultrapure water

6.2.1.2 Weigh out 0.1 g Uranyl formate (UFo) into a 15 mL conical tube.

6.2.1.3 Add 5 mL of the hot water to UFo powder for a 2% solution. Close tightly and wrap in aluminum foil to block light. 1% Uranyl acetate stain is also commonly used.

6.2.1.4 Vortex or shake vigorously for 5 min. Fastening tube to the vortexer will help.

6.2.1.5 Filter through 0.2 µm syringe filter into a clean conical tube.

6.2.1.6 Let cool 10 min to room temperature.

6.2.1.7 Add 25 µL of 5M NaOH and vortex immediately for 2 min.

6.2.1.7.1 Alternatively, freeze 200 µL aliquots of 2% UFo. When ready for use, thaw aliquot, add 1 µL of 5M NaOH, and vortex for 2 min.

6.2.1.8 Keep stain wrapped in foil or away from light.

6.2.2 Dilute sample 10x in 1x PBS (or desired buffer).

6.2.3 Select grid. We recommend carbon support film on copper grids. The darker shinier side of the grid is the carbon-coated side where you will deposit and stain your sample.

6.2.4 Place grid carbon-side up in a glow discharging apparatus on a clean glass slide. See Step 6.1.2.

6.2.5 Expose grid for 30 s.

6.2.6 Pick up grid with the carbon side still facing up and hold with negative action tweezers by the edge of the grid to prevent tearing the imaging area in the center. Set down the tweezers with the grid still held carbon-side up.

6.2.7 Apply a 4 µL droplet of sample to the top (carbon side) of the grid with a pipette.

6.2.8 Incubate 4 min.

6.2.9 With ~1 min left, pipette a 10 µL and a 20 µL drop of UFo solution onto a piece of clean laboratory film

6.2.10 Use filter paper to wick the sample from grid from the edge of the grid (perpendicular contact) to avoid any contact with the imaging surface.

6.2.11 Using the tweezers (still holding the grid), immediately place the sample side of the grid down on the 10 µL UFo droplet then immediately wick off the liquid (wash step). It is important not to let grid fully dry during these steps so do not stop in between steps.

6.2.12 In a similar manner, apply the 20 µL UFo droplet to the grid. Hold the grid on the UFo for 40 s. Wick the liquid off and let the grid dry.

6.2.13 Image dry grid at 120 kV between 20kx and 100kx.

6.2.14 Be sure to properly dispose of all UFo-contaminated materials through the institution's safety service for radioactive waste.

6.2.15 When necessary, brightness/contrast enhancement and a median filter can be applied to TEM images in ImageJ to reduce background noise. Post processing should be done uniformly, only for images that are not utilized for quantitative measurements such as intensity, and should always be reported.

Representative Results

In order to illustrate the characterization methods described above, we show typical results for PCMs assembled from oligonucleotides and block copolymers of various lengths and chemistries (cartoon schematic in Figure 1). Figure 2 provides an example of how PCM core size (as determined from SAXS and TEM, Figures 4 and 5) varies with charged block length. Figure 3 shows DLS data and fitting results for spherical PCMs formed from relatively long block copolymers and short single-stranded oligonucleotides. Figure 4 illustrates how complex SAXS intensity spectra can be accurately fit by combining models for the multiple spatial correlations that are present (external surface, intra-core scattering, inter-helix ordering), and how MALS can be used to extend scattering measurements to longer length scales. Finally, Figure 5 shows representative electron microscopy data for PCMs of varying morphology.

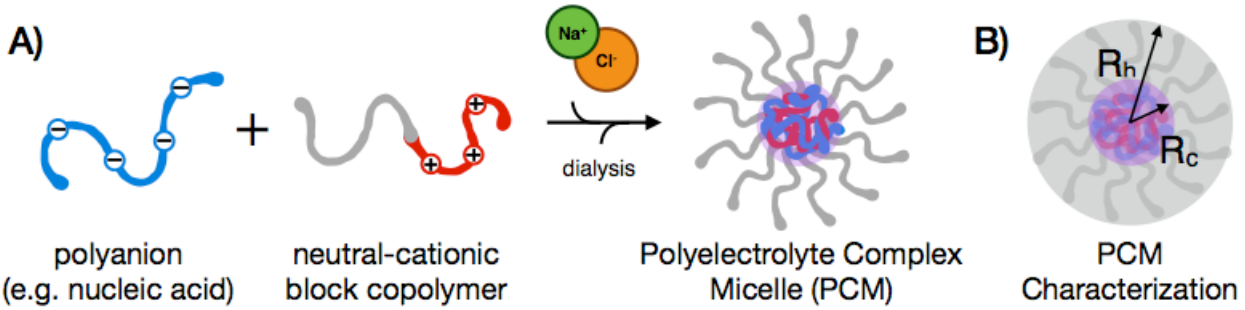

Figure 1: Assembly and Characterization of nucleic acid PCMs. (A) Anionic polymers, such as oligonucleotides, form phase-separated complexes with cationic regions of diblock copolymers. The presence of a hydrophilic neutral block (gray) results in formation of stable PCM nanoparticles. (B) PCMs are core-shell nanoparticles with multiple parameters to characterize. The overall size (hydrodynamic radius, R_h) can be determined using DLS, the core radius (R_c) can be found using SAXS and TEM, corona size can be calculated as R_h-R_c, and morphology can be determined over multiple length scales by combining SAXS, MALS, and TEM.

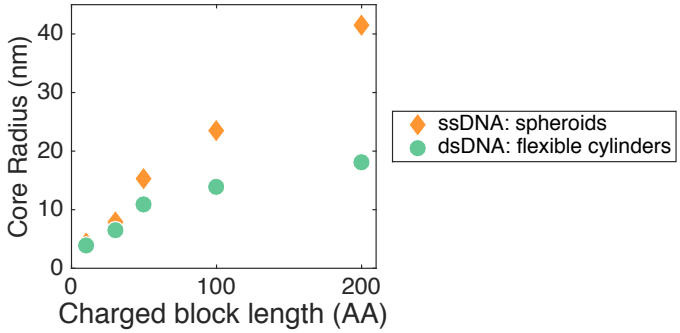

Figure 2: Micelle Size Dependence. Micelle core size is primarily determined by the length of the charged block of the block copolymer, and largely independent of the length of the homopolymer[7,26]. This allows for control of PCM size by choice of block polymer. The data shown here is for pLys-PEG with 88 nt/bp DNA and has been previously reported[26].

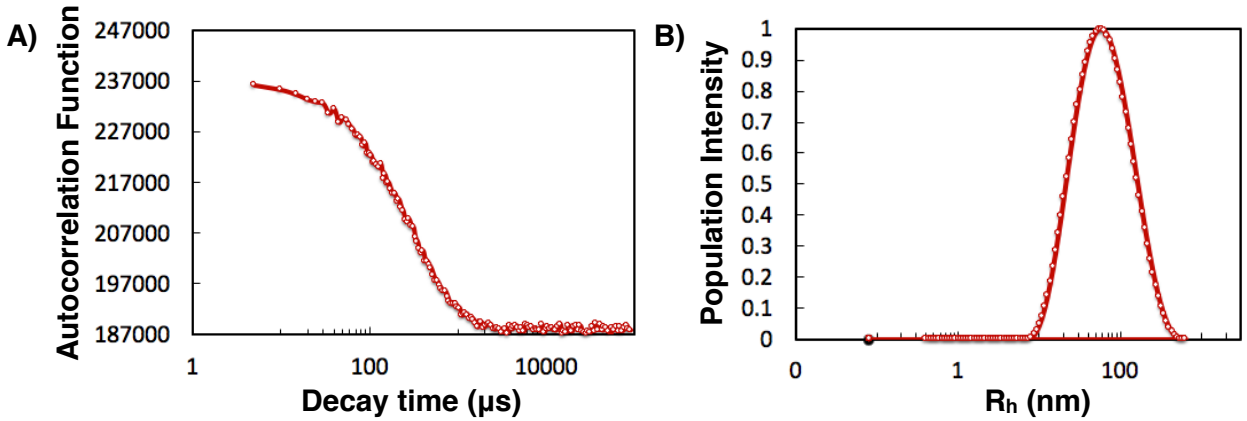

Figure 3: Dynamic Light Scattering. (A) Autocorrelation function (arbitrary units) for 10 nt single-stranded DNA + pLys(100)-PEG(10k) PCM. (B) Hydrodynamic radius distribution (histogram) from REPES fit. The autocorrelation function decays to a flat value with a single time scale, resulting in a single size peak in the REPES size distribution.

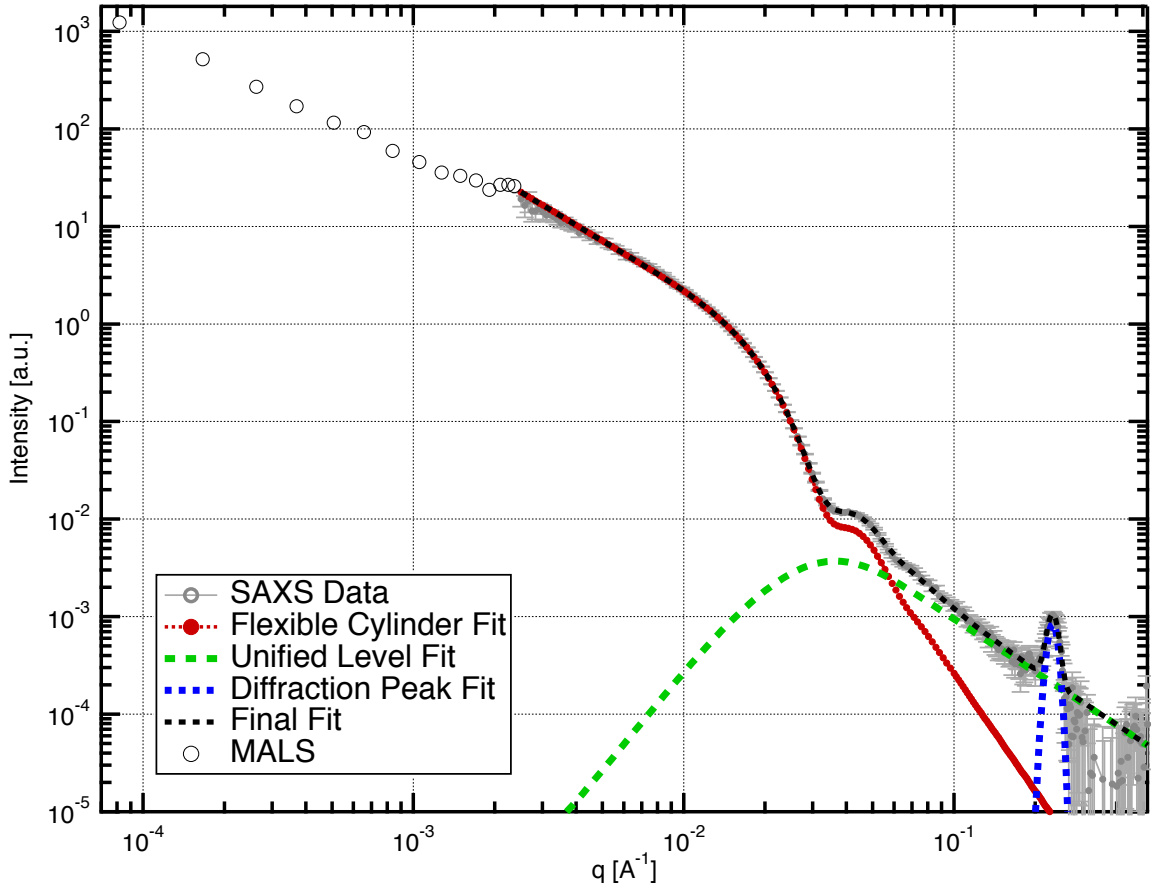

Figure 4: Representative SAXS and MALS data and fit for a cylindrical micelle. SAXS data (gray circles) is shown for PCMs assembled from pLys(50)-PEG(5k) and 88 bp double-stranded DNA. At low q (< 10^{-2} Å^{-1}), the intensity shows an approximately q^{-2} dependence on momentum transfer, implying a flexible cylinder shape (worm-like micelle). MALS data (open black circles) shows the same dependence, indicating the micelles are at least several μm in length (corroborated by TEM imaging, Figure 5c,d). Spheroidal micelles would show a flat dependence (q^0) of intensity on q in this range. The colored lines illustrate the multi-component fitting procedure for PCM SAXS data described in

Section 5. Scattering at low-q (large distance scales) is dominated by the external surface of the PCM, and is fit well by a flexible cylinder model (red). At higher q values (smaller length scale), scattering is dominated by the individual polymers inside the PCM core, fit here by a power law (green) with low q cutoff. We also observe parallel packing of double-stranded DNA helices within the PCM core, resulting in a quasi-Bragg diffraction peak (blue). The black dashed line shows that combining these models accurately describes the SAXS data, and the addition of light-scattering data (open circles) extends the size range over nearly 4 orders of magnitude. Fitting results give a PCM population with Mean Radius = 11.0 nm and PDI=0.03, power law at high q of 1.81 and the diffraction peak represents inter-helix spacing of 2.71 nm. SAXS data has been previously reported[26] and is publicly available[44].

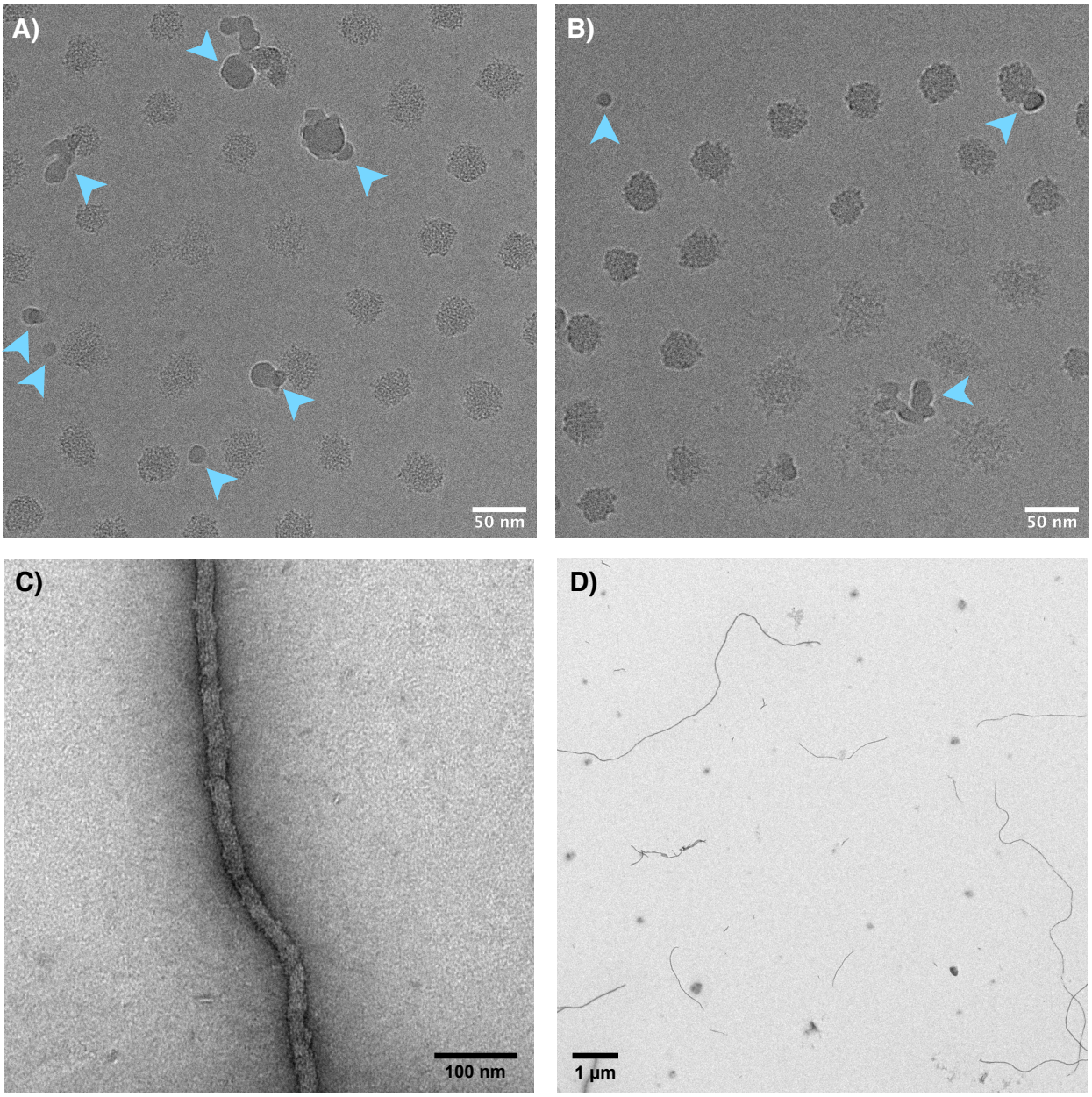

Figure 5: TEM images of nucleic acid PCMs. (A-B) Cryo TEM of 22 nt single-stranded DNA + pLys(50)-PEG(5k) PCMs, showing predominantly spherical morphology. Blue arrows indicate liquid ethane droplets, not to be confused with the PCMs (textured spheroidal objects). (A) is slightly under-

focused, adding slight contrast while preserving resolution. (B) is substantially under-focused, adding more contrast but sacrificing clarity. Brightness and contrast adjustments and a 2 pixel median filter were applied to both images. (C-D) Negative stained TEM of 88 bp double-stranded DNA + pLys(50)-PEG(5k) PCMs, which are long flexible cylinders. In both cases, core radii from TEM are consistent with the values obtained from fitting SAXS data.

Discussion

As mentioned above, the protocols presented here are written with a focus on oligonucleotides as the polyanion component and pLys-PEG as the cationic-neutral block copolymer, but we have tested them with a variety of polymers (e.g. poly(acrylic acid), poly(glutamate), PEG-poly(vinylbenzyl trimethylammonium), etc.) and believe they will be generally applicable for most polyelectrolyte pairs. One parameter that may need to be experimentally optimized is the salt concentration used for annealing: it should be high enough that PCMs do not form at the beginning of the anneal. This can be checked experimentally by DLS, or by comparison to observation of phase separation with the polyelectrolytes alone (no neutral block). Thermal annealing can be used if salt annealing is undesirable, though the resulting polydispersities are larger[7]. The concentrations used for characterization also may need to be optimized; larger nanoparticles scatter more light than small ones, and nucleic acids are more efficient at scattering X-rays than many other polymers due to the presence of electron-dense phosphorus atoms in the backbone. It may also be necessary to more closely control the pH of the buffer if either polyelectrolyte has a pKa close to the working condition.

We present protocols for two light scattering techniques (multi-angle (static) light scattering and dynamic light scattering), small-angle X-ray scattering, and both cryo and conventional negative stain transmission electron microscopy in this article, with representative data for each. Not all techniques are necessary for all scenarios, and others are available as well, raising the question of which should be employed when. Ample review literature exists on this subject[45,46], but we suggest the following when characterizing a new PCM or similar nanoparticle. Begin by checking for aggregation, both by visual inspection for turbidity and by optical microscopy. If no aggregation is observed, the next step is to determine whether any nanoparticles exist. DLS is a quick way to determine this; PCMs scatter light vigorously, and weak or nonexistent light scattering is a strong indicator of poor nanoparticle formation. While DLS can confirm the presence of nanoparticles, it is difficult to determine their size and shape without reference to other data, as most analysis methods rely on the Stokes-Einstein relation which assumes spherical particles. MALS can confirm spherical shapes (flat normalized intensity vs angle) but may not be able to determine the shape of non-spherical particles unless the size distribution is both narrow and happens to fall in the correct range for resolution. As a result, we recommend performing TEM, SAXS, or both on any PCM sample in order to fully characterize its properties.

Acknowledgements

We thank Phil Griffin and Tera Lavoie of the Soft Matter Characterization Facility and Advanced Electron Microscopy Facility, respectively, at The University of Chicago. We

also thank Xiaobing Zuo and Soenke Seifert of the Advanced Photon Source at Argonne National Laboratory and NIST Center for Hierarchical Materials Design (CHiMaD) for support. We thank Jeff Ting and Michael Lueckheide for their contributions to this work.

References

1 Spruijt, E., Westphal, A. H., Borst, J. W., Cohen Stuart, M. A. & van der Gucht, J. Binodal compositions of polyelectrolyte complexes. *Macromolecules.* **43** (15), 6476-6484, (2010).

2 van der Gucht, J., Spruijt, E., Lemmers, M. & Cohen Stuart, M. A. Polyelectrolyte complexes: bulk phases and colloidal systems. *Journal of Colloid and Interface Science.* **361** (2), 407-422, (2011).

3 Priftis, D., Laugel, N. & Tirrell, M. Thermodynamic characterization of polypeptide complex coacervation. *Langmuir.* **28** (45), 15947-15957, (2012).

4 Fu, J. & Schlenoff, J. B. Driving Forces for Oppositely Charged Polyion Association in Aqueous Solutions: Enthalpic, Entropic, but Not Electrostatic. *Journal of the American Chemical Society.* **138** (3), 980-990, (2016).

5 Vieregg, J. R. *et al.* Oligonucleotide-Peptide Complexes: Phase Control by Hybridization. *Journal of the American Chemical Society.* **140** (5), 1632-1638, (2018).

6 Voets, I. K., de Keizer, A. & Cohen Stuart, M. A. Complex coacervate core micelles. *Advances in Colloid and Interface Science.* **147-148** 300-318, (2009).

7 Lueckheide, M., Vieregg, J. R., Bologna, A. J., Leon, L. & Tirrell, M. V. Structure-Property Relationships of Oligonucleotide Polyelectrolyte Complex Micelles. *Nano Letters.* **18** (11), 7111-7117, (2018).

8 De Kruif, C. G., Weinbreck, F. & de Vries, R. Complex coacervation of proteins and anionic polysaccharides. *Current opinion in colloid & interface science.* **9** (5), 340-349, (2004).

9 Vieregg, J. R. & Tang, T. Y. D. Polynucleotides in cellular mimics: Coacervates and lipid vesicles. *Current opinion in colloid & interface science.* **26** 50-57, (2016).

10 Marciel, A. B., Chung, E. J., Brettmann, B. K. & Leon, L. Bulk and nanoscale polypeptide based polyelectrolyte complexes. *Advances in Colloid and Interface Science.* **239** 187-198, (2017).

11 Cabral, H., Miyata, K., Osada, K. & Kataoka, K. Block Copolymer Micelles in Nanomedicine Applications. *Chemical Reviews.* **118** (14), 6844-6892, (2018).

12 Tan, Z. *et al.* Block Polymer Micelles Enable CRISPR/Cas9 Ribonucleoprotein Delivery: Physicochemical Properties Affect Packaging Mechanisms and Gene Editing Efficiency. *Macromolecules.* (2019).

13 Horn, J. M., Kapelner, R. A. & Obermeyer, A. C. Macro- and Microphase Separated Protein-Polyelectrolyte Complexes: Design Parameters and Current Progress. *Polymers.* **11** (4), (2019).

14 Juliano, R. L. The delivery of therapeutic oligonucleotides. *Nucleic Acids Research.* **44** (14), 6518-6548, (2016).

15 Kanasty, R., Dorkin, J. R., Vegas, A. & Anderson, D. Delivery materials for siRNA therapeutics. *Nature Materials.* **12** (11), 967-977, (2013).

16 Lorenzer, C., Dirin, M., Winkler, A. M., Baumann, V. & Winkler, J. Going beyond the liver: progress and challenges of targeted delivery of siRNA therapeutics. *Journal of Controlled Release.* **203** 1-15, (2015).

17 Allen, T. M. & Cullis, P. R. Liposomal drug delivery systems: from concept to clinical applications. *Advanced Drug Delivery Reviews.* **65** (1), 36-48, (2013).

18 Li, W. & Szoka, F. C., Jr. Lipid-based nanoparticles for nucleic acid delivery. *Pharmaceutical Research.* **24** (3), 438-449, (2007).

19 Miyata, K., Nishiyama, N. & Kataoka, K. Rational design of smart supramolecular assemblies for gene delivery: chemical challenges in the creation of artificial viruses. *Chemical Society Reviews.* **41** (7), 2562-2574, (2012).

20 Oishi, M., Nagasaki, Y., Itaka, K., Nishiyama, N. & Kataoka, K. Lactosylated poly(ethylene glycol)-siRNA conjugate through acid-labile ss-thiopropionate linkage to construct pH-sensitive polyion complex micelles achieving enhanced gene silencing in hepatoma cells. *Journal of the American Chemical Society.* **127** (6), 1624-1625, (2005).

21 Christie, R. J. *et al.* Targeted polymeric micelles for siRNA treatment of experimental cancer by intravenous injection. *ACS Nano.* **6** (6), 5174-5189, (2012).

22 Kuo, C. H. *et al.* Inhibition of atherosclerosis-promoting microRNAs via targeted polyelectrolyte complex micelles. *Journal of Materials Chemistry B.* **2** (46), 8142-8153, (2014).

23 Ge, Z. *et al.* Targeted gene delivery by polyplex micelles with crowded PEG palisade and cRGD moiety for systemic treatment of pancreatic tumors. *Biomaterials.* **35** (10), 3416-3426, (2014).

24 Van Bruggen, C., Hexum, J. K., Tan, Z., Dalai, R. J. & Reineke, T. M. Nonviral Gene Delivery with Cationic Glycopolymers. *Accounts of Chemical Research.* **52** (5), 1347-1358, (2019).

25 Hayashi, K. *et al.* Influence of RNA Strand Rigidity on Polyion Complex Formation with Block Catiomers. *Macromolecular Rapid Communications.* **37** (6), 486-493, (2016).

26 Marras, A. E., Vieregg, J. R., Ting, J. M., Rubien, J. D. & Tirrell, M. V. Polyelectrolyte Complexation of Oligonucleotides by Charged Hydrophobic-Neutral Hydrophilic Block Copolymers. *Polymers.* **11** (1), 83, (2019).

27 Phillips, H. R. *et al.* Glycopolycation–DNA Polyplex Formulation N/P Ratio Affects Stability, Hemocompatibility, and in Vivo Biodistribution. *Biomacromolecules.* **20** (4), 1530-1544, (2019).

28 Ting, J. M., Wu, H., Herzog-Arbeitman, A., Srivastava, S. & Tirrell, M. V. Synthesis and Assembly of Designer Styrenic Diblock Polyelectrolytes. *Acs Macro Letters.* **7** (6), 726-733, (2018).

29 Zadeh, J. N. *et al.* NUPACK: Analysis and design of nucleic acid systems. *Journal of Computational Chemistry.* **32** (1), 170-173, (2011).

30 SantaLucia, J., Jr. A unified view of polymer, dumbbell, and oligonucleotide DNA nearest-neighbor thermodynamics. *Proceedings of the National Academy of Sciences of the United States of America.* **95** (4), 1460-1465, (1998).

31 Xia, T. *et al.* Thermodynamic parameters for an expanded nearest-neighbor model for formation of RNA duplexes with Watson-Crick base pairs. *Biochemistry.* **37** (42), 14719-14735, (1998).

32 Orthaber, D., Bergmann, A. & Glatter, O. SAXS experiments on absolute scale with Kratky systems using water as a secondary standard. *Journal of Applied Crystallography.* **33** (2), 218-225, (2000).

33 Srivastava, S. *et al.* Gel phase formation in dilute triblock copolyelectrolyte complexes. *Nature Communications.* **8** 14131, (2017).

34 Lindhoud, S. *et al.* Salt-induced disintegration of lysozyme-containing polyelectrolyte complex micelles. *Langmuir.* **25** (19), 11425-11430, (2009).

35 Lindhoud, S., de Vries, R., Schweins, R., Stuart, M. A. C. & Norde, W. Salt-induced release of lipase from polyelectrolyte complex micelles. *Soft Matter.* **5** (1), 242-250, (2009).

36 Ilavsky, J. & Jemian, P. R. Irena: tool suite for modeling and analysis of small-angle scattering. *Journal of Applied Crystallography.* **42** (2), 347-353, (2009).

37 Sambrook, J., Fritsch, E. F. & Maniatis, T. *Molecular cloning: a laboratory manual*. (Cold spring harbor laboratory press, 1989).

38 Jakeš, J. Regularized positive exponential sum (REPES) program-A way of inverting laplace transform data obtained by dynamic light scattering. *Collection of Czechoslovak chemical communications.* **60** (11), 1781-1797, (1995).

39 Schillen, K., Brown, W. & Johnsen, R. M. Micellar Sphere-to-Rod Transition in an Aqueous Triblock Copolymer System - a Dynamic Light-Scattering Study of Translational and Rotational Diffusion. *Macromolecules.* **27** (17), 4825-4832, (1994).

40 Provencher, S. W. Contin - a General-Purpose Constrained Regularization Program for Inverting Noisy Linear Algebraic and Integral-Equations. *Computer Physics Communications.* **27** (3), 229-242, (1982).

41 Provencher, S. W. A Constrained Regularization Method for Inverting Data Represented by Linear Algebraic or Integral-Equations. *Computer Physics Communications.* **27** (3), 213-227, (1982).

42 Sarachan, K. L., Curtis, J. E. & Krueger, S. Small-angle scattering contrast calculator for protein and nucleic acid complexes in solution. *Journal of Applied Crystallography.* **46** (6), 1889-1893, (2013).

43 Beaucage, G. Approximations leading to a unified exponential power-law approach to small-angle scattering. *Journal of Applied Crystallography.* **28** (6), 717-728, (1995).

44 Marras, A. E., Vieregg, J. R., Ting, J. M., Rubien, J. D. & Tirrell, M. V. 10.18126/M2QW8R (Materials Data Facility, 2018).

45 Modena, M. M., Rühle, B., Burg, T. P. & Wuttke, S. Nanoparticle Characterization: What to Measure? *Advanced Materials.* 1901556, (2019).

46 Mourdikoudis, S., Pallares, R. M. & Thanh, N. T. K. Characterization techniques for nanoparticles: comparison and complementarity upon studying nanoparticle properties. *Nanoscale.* **10** (27), 12871-12934, (2018).